



Energetic ion enhancements in sheaths driven by interplanetary coronal mass ejections

Emilia Kilpua¹ · Rami Vainio² · Christina Cohen³ · Nina Dresing² · Simon Good¹ · Julia Ruohotie¹ · Domenico Trotta⁴ · Stuart D. Bale⁵ · Eric Christian⁶ · Matt Hill⁷ · David J. McComas⁸ · Ralph McNutt⁷ · Nathan Schwadron⁹

Received: 17 December 2022 / Accepted: 22 May 2023
© The Author(s) 2023

Abstract

We analyze here an energetic proton enhancement in a sheath ahead of a slow interplanetary coronal mass ejection (ICME) detected by Parker Solar Probe on June 30, 2021 at the heliospheric distance of 0.76 AU. The shock was likely quasi-parallel and had a high Mach number. However, the proton fluxes were not enhanced at the shock but about an hour later. The fluxes stayed elevated with a sporadic behaviour throughout the sheath. We suggest that some mechanism internal to the sheath was responsible for the energization. The observations show enhanced levels of magnetic field fluctuations in the sheath and frequent presence of highly reduced magnetic helicity structures (σ_m) at various time scales, representing either small-scale flux ropes or Alfvénic fluctuations that could have contributed to the energization. The correlation between the energetic proton fluxes and normalized fluctuation amplitudes/occurrence of high σ_m structures was generally weak or negligible. The most striking feature of the sheath was a strong enhancement of density (up to 50 cm^{-3}) that implies the importance of compressive acceleration in the sheath. A statistical analysis of ion enhancements of 73 sheaths detected by ACE at ~ 1 AU reveals that this sheath was peculiar as in ICME-driven sheaths preceded by strong shocks the ion fluxes typically peak at the shock and strongly decline through the sheath.

Keywords Particle acceleration · Solar wind · Interplanetary shocks · Coronal mass ejections

1 Introduction

The acceleration of charged particles to high energies is an intriguing fundamental and universal process that occurs ubiquitously in various space and astrophysical plasma environments (e.g., Retinò et al. 2021). In our solar system, solar energetic particles (SEPs, e.g., Reames 2013) pose also a significant threat to satellites in orbit and astronauts working in space, and they can also reach the Earth's upper atmosphere affecting its composition and dynamics (e.g., Vainio et al. 2009; Krivolutsky and Repnev 2012; Desai and Giacalone 2016). The details of how charged particles are energised are, however, not fully understood.

Energetic particles are known to be accelerated at high Mach number shocks driven by coronal mass ejections (CMEs; Webb and Howard 2012) and their interplanetary counterparts (ICMEs; Kilpua et al. 2017) via diffusive shock acceleration (DSA; e.g., Giacalone 2012). In the classic DSA picture, particles efficiently gain energy by crossing

the shock multiple times, scattering from upstream to downstream due to magnetic field irregularities generated on the upstream side of the shock by the accelerated particles themselves (e.g., Afanasiev et al. 2015, 2018). This process, known as first-order Fermi acceleration, is expected to be most efficient for quasi-parallel shocks that have a high level of self-induced upstream/downstream fluctuations. Energetic particles are, however, also associated with relatively slow CMEs in the corona that have low Mach number shocks (magnetosonic Mach number < 2) or even no shock at all, i.e., their inferred Mach numbers are below 1 (e.g., Kouloumvakos et al. 2019; Giacalone et al. 2020). Recent observations have also related energetic ion enhancements to low Mach number ICME-driven shocks in interplanetary space (e.g., Giacalone et al. 2020; Kilpua et al. 2021b). These studies suggest that additional acceleration mechanisms to DSA could significantly contribute to particle energization at coronal and interplanetary shock waves.

One option is that the compressed and turbulent sheath following the shock (e.g., Kilpua et al. 2017) would have in some cases a key role in accelerating charged particles (e.g.,

Extended author information available on the last page of the article

Manchester et al. 2005; Kilpua et al. 2021b; Schwadron et al. 2020). Even slow ICMEs preceded by weak shocks are known to have prominent sheaths with high densities and magnetic field fluctuation levels enhanced relative to the preceding wind (Kilpua et al. 2019, 2020, 2021a). The event studied by Giacalone et al. (2020) was observed in-situ at the distance of 0.25 AU from the Sun by Parker Solar Probe (PSP; Fox et al. 2016). In that case, the authors deduced that the detected enhancement was a remnant from the acceleration that had occurred closer to the Sun by a weak coronal shock that had dissipated by the time it reached the PSP location. In the event analyzed by Kilpua et al. (2021b) at distances ~ 0.8 –1 AU from the Sun the energization was related to small-scale coherent structures that were likely swept from the upstream solar wind to the sheath, namely a warp in the heliospheric current sheet (HCS) and small-scale magnetic flux rope that was compressed at the leading edge of the ICME ejecta. Another interesting recent event was the series of CMEs/ICMEs analyzed by Schwadron et al. (2020) that occurred on 18–24 April 2019 when PSP was ~ 0.48 AU from the Sun. One of these ICMEs intercepted PSP and enhancements in energetic particle fluxes were interpreted to result from the acceleration by the compressed sheath ahead of the ICME rather than from DSA.

In this paper we investigate a substantial enhancement of energetic protons during a sheath preceding an ICME detected by PSP on June 30 – July 1, 2021 when it was at the distance of ~ 0.76 AU from the Sun. The proton fluxes were not enhanced immediately at the shock, but approximately an hour later in the sheath and the fluxes stayed elevated throughout the sheath. It is, therefore, expected that some process internal to the sheath was responsible for the energization in this case. To gain a deeper insight into how common such enhancements are in sheaths, a statistical analysis is conducted over 73 sheaths detected by the ACE spacecraft at 1 AU. The paper is organized as follows: Sect. 2 will first introduce the data sets used, Sect. 3 presents the results and Sects. 4 and 5 discuss and conclude.

2 Data

The case study presented here uses observations from the Parker Solar Probe. The magnetic field measurements are obtained from the FIELDS instrument (Bale et al. 2016). We use both 1-minute resolution data to capture the overall characteristics of the event and the high-resolution magnetic field data of 0.128-s resolution to study magnetic field fluctuations. The plasma data comes from the Solar Wind Electrons Alphas and Protons (SWEAP) instrument suite (Kasper et al. 2016). The data resolution of the processed data for the investigated interval is ~ 27 sec. We use here plasma data only for discussing global features of the sheath and do not conduct any detailed analysis based on them.

The PSP energetic ion measurements come from the Integrated Science Investigation of the Sun (ISoIS McComas et al. 2016). We use here the data from the Energetic Particle Instrument-Low (EPI-Lo Hill et al. 2017, 2020) that measures the lower energy particles. The instrument provides observations of ions from ~ 20 keV to 15 MeV/nucleon total energy.

The statistical analysis uses energetic ion observations from the Advanced Composition Explorer (ACE; Stone et al. 1998) spacecraft's Electron, Proton and Alpha Monitor (EPAM; Gold et al. 1998) instrument.

3 Results

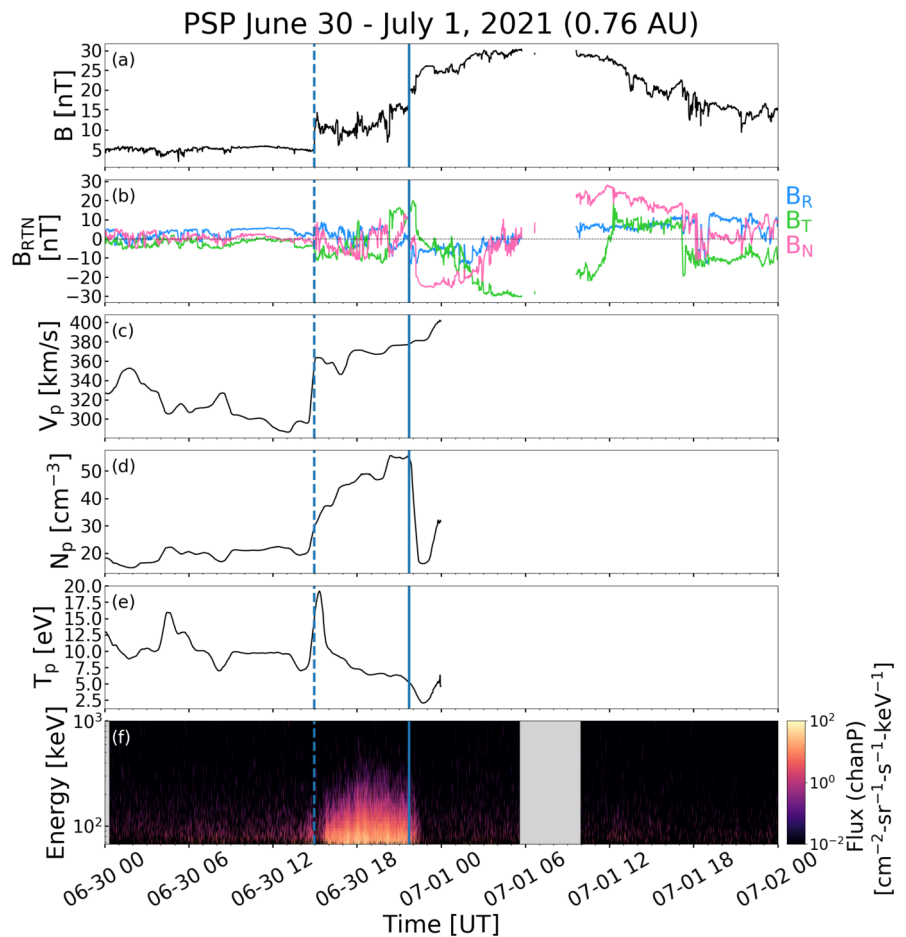
3.1 Event overview

The analyzed ICME was observed by PSP at the heliospheric distance of 0.76 AU from the Sun on June 30 – July 1, 2021. Figure 1 shows the magnetic field, plasma and energetic proton data from PSP during this period. First, the observations indicate an interplanetary shock (dashed blue vertical line) on June 30th at 14:58:20 UT as seen by the simultaneous jumps in the magnetic field magnitude, speed, temperature and density. Another prominent feature in Fig. 1 is an extended period of elevated magnetic field up to about 30 nT coinciding with a coherent rotation of the magnetic field Radial Tangential Normal (RTN) components. These are signatures of a magnetic cloud (e.g., Burlaga et al. 1981) that are a subset of ICMEs. Their characteristic features are believed to be an indication of the flux rope morphology (e.g., Kilpua et al. 2017). The leading edge of the magnetic cloud is marked at June 30 at 21:48 UT (solid blue vertical line) at the point where the coherent field rotation starts and solar wind density drops drastically. The end time of the ICME is ambiguous and it is not marked in the figure.

The sheath region is located between the shock and the magnetic cloud leading edge and it lasted 7.2 hours. Figure 1 shows that magnetic field fluctuations are enhanced in the sheath, but the magnetic field magnitude is considerably lower than in the cloud, up to about 10–12 nT, but nevertheless clearly enhanced with respect to the preceding value due to the interplanetary shock. The solar wind density is, however, strongly enhanced in the sheath with respect to the upstream wind, increasing from 15–20 cm^{-3} upstream of the shock to over 50 cm^{-3} at the magnetic cloud leading edge.

The last panel of Fig. 1 shows the proton flux spectrogram from the PSP EPI-Low instrument. The plot shows a clear enhancement of protons at energies from ~ 80 keV to ~ 300 keV. This enhancement occurs solely in the sheath and starts about an hour after the shock. The energies of this enhancement are typical to those observed in slow-fast

Fig. 1 Magnetic field, plasma and energetic ion observations during the ICME event on June 30 – July 1, 2021 as observed by PSP at 0.76 AU distance from the Sun. From top to bottom, we show a) the magnetic field magnitude, b) three magnetic field components in RTN (blue: B_R , green: B_T , pink: B_N), c) solar wind speed, d) density, e) temperature, and f) the spectrogram of proton flux intensity versus energy and time from channel P of EPI-Low. The dashed blue vertical line marks the shock and solid blue vertical line the ejecta leading edge. Note that the plasma data is missing soon after the sheath ends due to the SWEAP data gap



stream interaction regions at the orbit of the Earth (SIRs; e.g., Richardson 2018). As the proton flux enhancement starts well after the shock it is likely that the sheath, not the shock, has the key relevance for energising the protons in this event.

3.2 Shock analysis

A zoom-in around the shock with high-resolution magnetic field data is shown in the left part of Fig. 2. Both the upstream and the downstream of the shock are characterised by large amplitude field fluctuations and variable field magnitude with the amplitudes being large in the downstream. According to Fig. 1 the solar wind speed jumps at the shock by about 50–60 km/s and the field from ~ 5 to ~ 11 nT.

The quality and cadence of the plasma data does not allow using them in the determination of the shock normal and in the calculation of the key shock parameters such as the shock speed and shock Mach numbers. The upstream field magnitude ~ 5 nT and density ~ 20 cm^{-3} give the upstream Alfvén speed of ~ 24 km/s, which is a relatively low value. For example, in the Heliospheric Shock Database (Kilpua et al. 2015) the mean upstream Alfvén speed for shocks detected at Wind is 56.3 ± 38.1 km/s. Since the shock strength

is determined by the ratio of the shock speed along the shock normal in the shock frame of reference to the upstream Alfvén speed, the low Alfvén speed implies that the shock investigated could be relatively strong despite the modest speed jump at the shock.

We estimated the shock normal using the magnetic field coplanarity method (see, e.g., Kilpua et al. 2015), systematically varying the upstream and downstream averaging intervals from 1 to 3 minutes in bins of 5 seconds, with the method introduced in Trotta et al. (2022b). The mean shock normal obtained was $\langle \mathbf{n}_{sh} \rangle = [0.94 \pm 0.019, 0.27 \pm 0.028, 0.17 \pm 0.070]$, i.e. the angle between the shock normal and radial direction from the Sun was small. This suggests that the ICME complex (comprising the shock, sheath and ejecta) was crossed close to the apex.

The estimates for the shock angle, i.e. the angle between the shock normal and the upstream magnetic field direction, are shown in right part of Fig. 2. The shock angle values were calculated using normals for 1–3 minute upstream and downstream intervals. The mean value is $35.6^\circ \pm 1.43^\circ$, i.e. the shock is quasi-parallel. The estimation of the shock being quasi-parallel is robust also when longer (~ 30 minutes) averaging windows are used. To estimate the Alfvén Mach

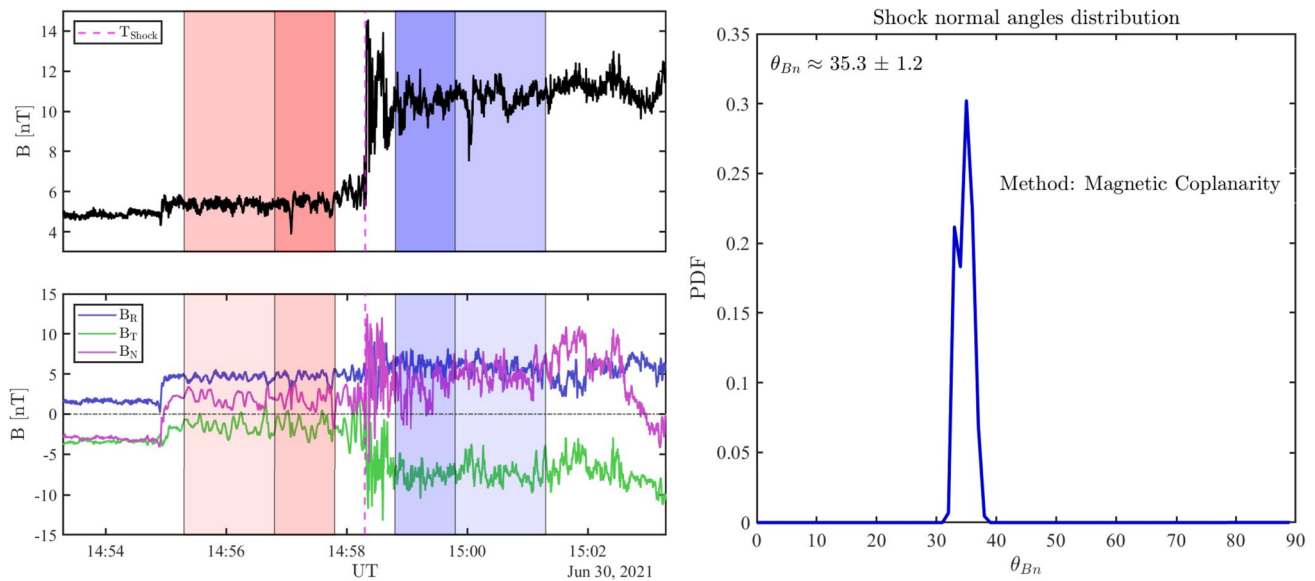


Fig. 2 Left) Magnetic field observations around the shock observed at PSP on June 30, 14:58:20 UT. The top panel gives the magnetic field magnitude and the bottom shows the magnetic field components in RTN. The red (purple)-shaded regions show the maximum and min-

imum upstream (downstream) intervals that were used to calculate the shock normal. Right) PDF distribution of the shock normal angle values

number and magnetosonic Mach number we use the upstream average speed and density calculated for the maximum upstream interval of 3 minutes used in the shock normal calculation. This gives the shock speed 485.5 km/s and Alfvén Mach number 8.5 and magnetosonic Mach number 5.9. These values have large uncertainties, but based on the discussion above we can conclude that most likely this shock is quasi-parallel and supercritical with Mach number > 2 .

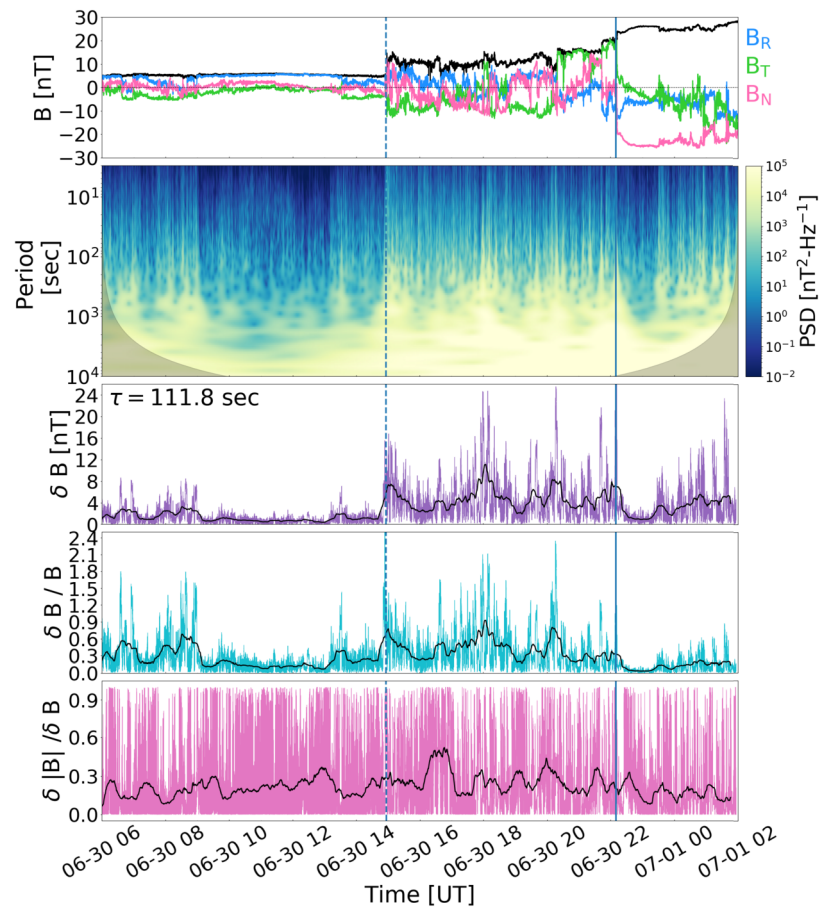
To get insight into the shock dynamics we evaluate both upstream and downstream the proton gyro frequency $\omega_c = (eB)/m_p$, where e is the elementary charge, B the magnetic field magnitude and m_p proton mass, and the proton inertial length $d_i = c/\omega_p$, where c is the speed of light and $\omega_p = \sqrt{(n_p e^2)/(\epsilon_0 m_p)}$ the proton plasma frequency, where n_p is the proton density and ϵ_0 vacuum permittivity. The mean values and standard deviations of gyro frequencies calculated over 15 minute interval upstream and downstream are $0.45 \pm 0.00134 \text{ s}^{-1}$ and $1.05 \pm 0.116 \text{ s}^{-1}$, and ion inertial lengths are $45.4 \pm 1.55 \text{ km}$ and $40.1 \pm 0.678 \text{ km}$, respectively. The proton gyroperiods ($2\pi/\omega_c$) are ~ 14.1 and 6.03 seconds upstream and downstream, respectively, consistent thus approximately with the foot and overshoot domains of the shock visible in Fig. 2. The multispacecraft observations with varying spacecraft separation of $\sim 1 - 100 d_i$ have shown that interplanetary shocks can have drastically different magnetic field profiles and shock normals on separations over $5 d_i$ (Kajdič et al. 2019) suggesting highly irregular shock fronts, as also elucidated by self-consistent simulations (Preisser et al. 2020; Kajdič et al. 2021). For

the presently studied event this corresponds to distances $\gtrsim 200 - 250 \text{ km}$. Such ripples in the shock front could contribute to particle acceleration at the shocks that does not occur immediately at the shock (e.g., Hietala et al. 2009; Sundberg et al. 2016; Trotta and Burgess 2019). As discussed in the previous section the proton enhancement did not start not until about 60 minutes from the shock. This downstream interval corresponds to the width of $\sim 1.3 \times 10^6 \text{ km}$, i.e. $\sim 3.2 \times 10^4 d_i$ (using the average speed of 359.8 km/s) and therefore is much larger than expected sizes of ripples sizes and their effects.

3.3 Sheath analysis

Next, we will analyze those aspects of the sheath that could contribute to the energization of protons and possible acceleration mechanisms. Figure 3 shows a zoom-in to the sheath. The magnetic field magnitude and RTN components are repeated in the top panel. The second panel shows the wavelet spectrogram of total Power Spectral Density (PSD), i.e. trace PSD, of magnetic field fluctuations from 1 second to ~ 2.7 hours (corresponding frequency range $\sim 0.1 \text{ mHz} - 1 \text{ Hz}$). The last three panels give information of the magnetic field fluctuations, and are the fluctuation amplitude, normalized fluctuation amplitude and the compressibility of fluctuations. We define the fluctuation amplitudes as $\delta\mathbf{B} = \mathbf{B}(t) - \mathbf{B}(t + \tau)$ where τ denotes the timescale (or time lag) of fluctuations. The normalized fluctuation amplitude is defined as $\delta B/B$, where $\delta B = |\delta\mathbf{B}|$, B is the magnetic field magnitude calculated as the mean over the fluctuation (i.e.,

Fig. 3 PSP magnetic field and plasma observations between June 30 – July 1, 2021. The panels show from top to bottom): magnetic field magnitude and magnetic field components in RTN coordinates (blue: B_R , green: B_T and pink: B_N), the wavelet PSD of magnetic field fluctuations in the periods of 1 s to 2 hrs (~ 0.1 mHz – 1 Hz frequency range), fluctuation amplitude, normalized fluctuation amplitude and the compressibility of fluctuations. In the three bottom panels the time lag used to calculate fluctuation amplitude and compressibility is 111.8 seconds. The black curve shows the 15-minute sliding window average and the colored curves the 1-second values



over the chosen time scale τ , in Fig. 3 selected to be 118.8 sec.), and compressibility is $\delta|\mathbf{B}|/\delta B$. In Fig. 3 both one-second values (coloured lines) and the 15-minute sliding window averages (black solid lines) are shown. The chosen time lag is $\tau = 111.8$ seconds that corresponds in the inertial (MHD) range fluctuations.

The wavelet PSD of the magnetic field and the fluctuation amplitudes δB show higher values in the sheath when compared to the upstream. In particular, there is an interval of distinctly smoother magnetic field upstream of the shock extending from June 30 8:59 UT to 13:32 UT, i.e. ending approximately 76 minutes before the shock. The δB values also vary considerably within the sheath. There is no obvious trend, but the highest values occur in the middle of the sheath. The normalized fluctuation amplitudes ($\delta B/B$) are also enhanced in the sheath, but at more similar levels compared to the beginning of the upstream interval shown. The compressibility of fluctuations ($\delta|\mathbf{B}|/\delta B$) does not in turn vary drastically between the sheath and the surroundings.

Figure 4 compares in more detail the variations in proton fluxes to variations in normalized fluctuations amplitudes and compressibility of fluctuations in the sheath. The figure shows the values as 1-minute averages. Three energy channels (232.4, 123.0 and 82.5 keV) and two time lags (0.436

and 111.8 seconds) for $\delta B/B$ and $\delta|\mathbf{B}|/\delta B$ are selected. Firstly, it is also clear from this plot that the shock itself does not lead to any immediate energization of energetic proton fluxes. The fluxes start to increase only about one hour after the shock passage and stay enhanced until the end of the sheath. The enhancement shows a sporadic nature. There is no obvious one-to-one correspondence between flux variations and variations in $\delta B/B$ or $\delta|\mathbf{B}|/\delta B$, but the bursts in $\delta B/B$ at the mid-sheath and in the trailing part of the sheath coincide with the enhancements of 123.0 and 82.5 keV fluxes.

The left part of Fig. 5 shows the correlation between the proton fluxes and normalized fluctuation amplitudes. The colors show the values of the Pearson correlation between these two quantities. The ion fluxes include energy channels from 64.7 keV to 263.1 keV and normalized fluctuation amplitudes are calculated for time lags from 0.436 to ~ 890 seconds. The correlations or anti-correlations are negligible (< 0.20) or weak (< 0.40). The highest positive correlations (~ 0.35) occur at the energies around 100 keV and for the time lags $\gtrsim 100$ seconds.

The bottom panel of Fig. 4 shows the normalized reduced magnetic helicity (σ_m) calculated for time scales from 100 seconds to 2.7 hours (10^{-2} to 10^{-4} Hz). This quantity is a measure of rotation in the magnetic field and can be calcu-

Fig. 4 The panels show from top to bottom: PSP magnetic field magnitude and RTN components, the spectrogram of proton flux intensity versus energy and time from channel P of EPI-low, 5-minute averaged proton fluxes at three selected energy channels (232.4, 123.0 and 82.5 keV), 5-minute averaged normalized fluctuation amplitudes ($\delta B/B$) and compressibility of fluctuations ($\delta|\mathbf{B}|/\delta B$) at time lags $\tau = 0.436$ and $\tau = 111.8$ seconds, the spectrogram of normalized reduced magnetic helicity (σ_m). In the bottom panel the contours show $|\sigma_m| > 0.7$ regions

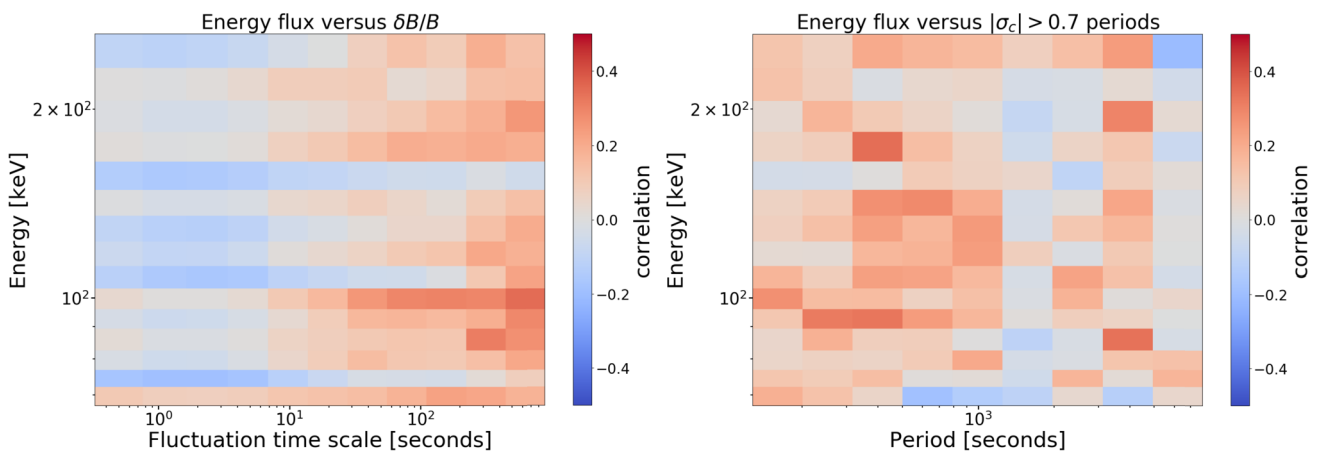
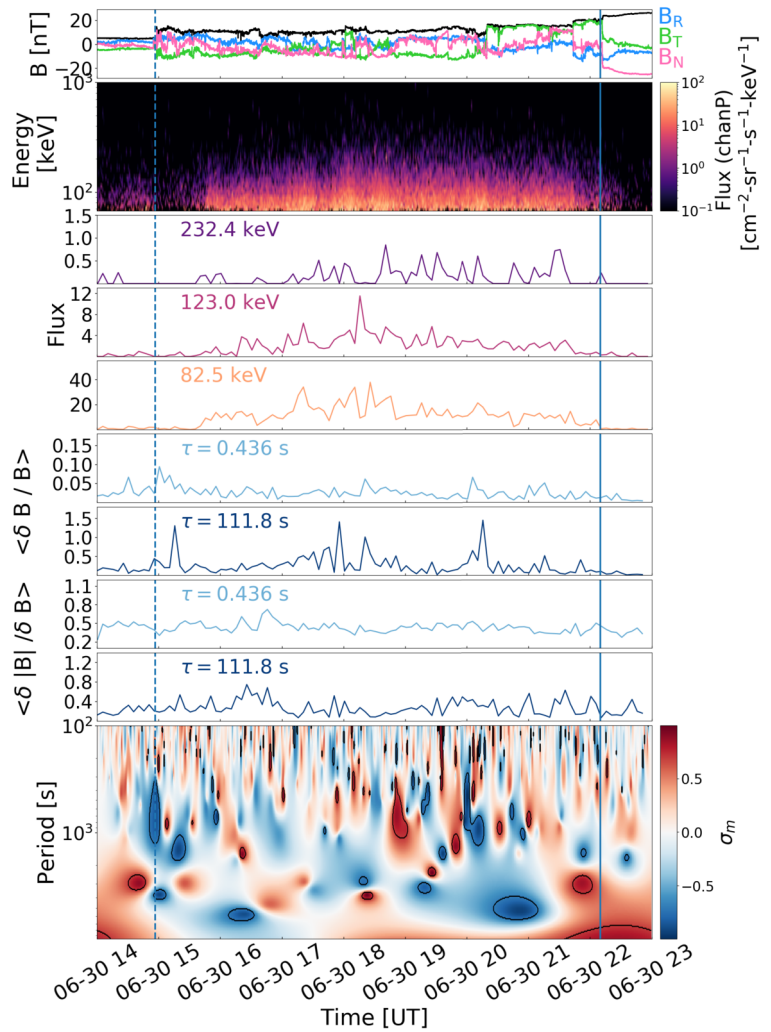


Fig. 5 Left) The colormap shows the Pearson correlation values between the 5-minute averages of proton fluxes and normalized fluctuation amplitudes calculated in the sheath for energy ranges from 64.7 keV to 263 keV, and time scales from 0.436 seconds to ~ 890

second. Right) the colormap shows the Pearson correlation values between the 5-minute averages of proton fluxes and occurrence of high normalized helicity ($|\sigma_m| > 0.7$) regions for periods from 100 seconds to ~ 2.7 hours

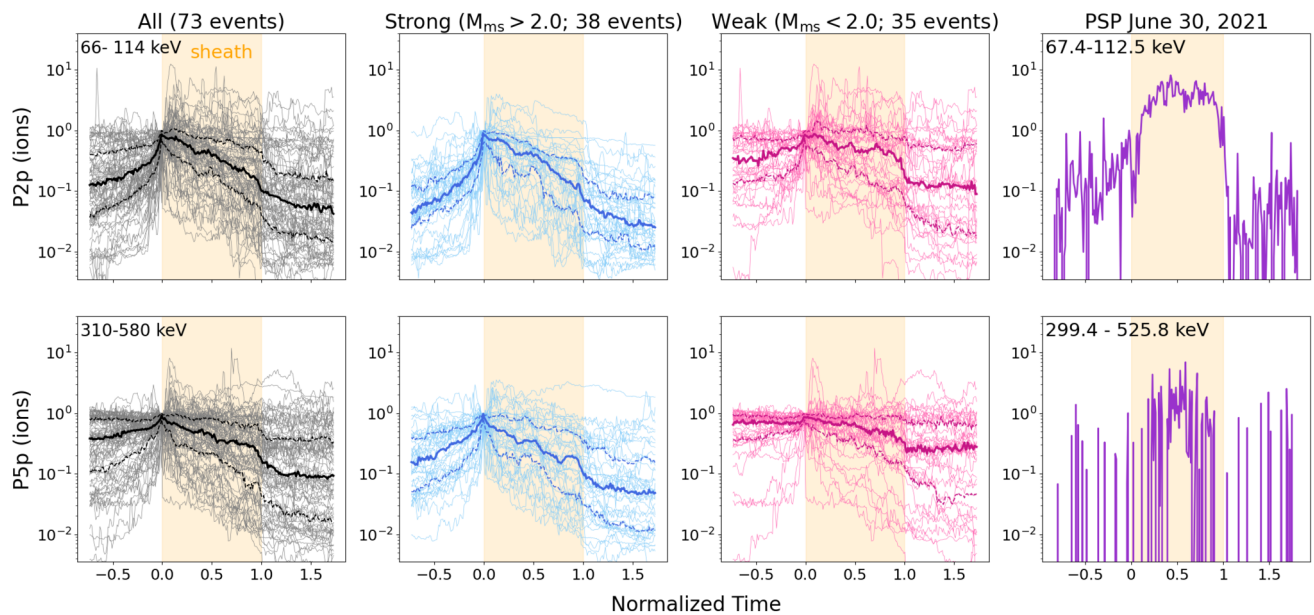


Fig. 6 A superposed epoch analysis of ion intensities during 73 sheath regions observed by the ACE satellite at the Lagrangian point L1, i.e., at ~ 1 AU distances from the Sun. The panels on the left show the results for all events, middle panels for strong shocks (magnetosonic Mach number > 2.0) and right panels for weak shocks (magnetosonic Mach number < 2.0). The thick curves give the medians and dashed

curves the lower and upper quartiles. The sheath interval has been indicated by the orange-shaded regions and all sheaths have been resampled to the same duration. The panels on the right show the averaged intensities at corresponding energy channels for the 30 June 2021 event analysed in Sect. 3.3

lated as (Matthaeus et al. 1982):

$$\sigma_m = \frac{2 \operatorname{Im} [W_T^*(\nu, t) \cdot W_N(\nu, t)]}{|W_R(\nu, t)|^2 + |W_T(\nu, t)|^2 + |W_N(\nu, t)|^2}, \quad (1)$$

where ν is the frequency of the associated wavelet function, and $W_R(\nu, t)$, $W_T(\nu, t)$, and $W_N(\nu, t)$ are the wavelet transforms of the magnetic field components in RTN coordinates. Normalized reduced magnetic helicity is one of the parameters that has been used to identify small-scale flux ropes from the solar wind together with normalized cross-helicity and residual energy (e.g., Zhao et al. 2020, 2021; Ruohotie et al. 2022). Due to the lack of high-resolution plasma data we were only able to calculate σ_m here. The black contours show $|\sigma_m| > 0.7$, i.e. the regions that have high magnetic helicity of either positive or negative sign and could represent small-scale flux ropes or circularly polarized low-frequency Alfvén waves. For the investigated event, Fig. 4 shows that from periods $\lesssim 1000$ seconds high- $|\sigma_m|$ regions occur sporadically throughout the sheath. Most larger-scale, high- $|\sigma_m|$ regions are identified near the shock and in the trailing part of the sheath.

The right part of Fig. 5 shows the correlations between the 5-minute averaged proton fluxes and the occurrence of $|\sigma_m| > 0.7$. Regarding σ_m , the spectrogram was divided in 10 period bins between 100 seconds to 2.7 hours. For each of these 10 bins we determined the fraction of when $|\sigma_m| > 0.7$ and calculated the 5 minutes averages. The correlations and

anti-correlations are again negligible or weak. The highest positive correlations (~ 0.40) occur at periods from a few hundreds to ~ 1000 seconds (i.e. from a few minutes to ~ 15 minutes) for a wide range of energies.

3.4 Statistical analysis

To get further insight as to whether enhancements of ion/proton fluxes are common in ICME-driven sheaths, we performed a statistical analysis of ACE measurements. This part of the study includes 73 sheaths that were selected from our previous studies (Kilpua et al. 2021a) to include those events that had ACE ion flux measurements available (list in the Appendix) observed during 1997 - 2017 at the Lagrangian point L1, i.e. ~ 1 AU distance from the Sun. The events are divided according to the shock magnetosonic Mach number to super- and subcritical cases $M_{ms} > 2$ and $M_{ms} < 2$. The duration of sheaths can vary considerably. For the included set they were between 3.4 and 21.8 hours with the mean duration 8.2 hours. To obtain the overall trend, all sheaths have been linearly rescaled to the same duration. The ion fluxes were normalised to the maximum flux in the 30 minute window around the shock.

The results are shown in the three first columns of Fig. 6 for ions in two energy channels (66–114 keV and 310–580 keV). The thick solid curve shows the population median and dashed thick curves the lower and upper quartiles. Individual curves are shown as thin lines. As expected,

the shock has an immediate and clear enhancing effect on the ion fluxes for the majority of $M_{ms} > 2$ cases (middle panels). Fluxes also increase at the shock for the $M_{ms} < 2$ cases (right panels), but the effect is much less pronounced. Another clear difference between the $M_{ms} > 2$ and $M_{ms} < 2$ cases is that for weak shocks ($M_{ms} < 2$), the median and in particular the upper quartile curves are flatter than for stronger shocks ($M_{ms} > 2$), in which the curves tend to decline from the shock through the sheath. This could imply a significant contribution from the sheath to the ion energization, particularly for sheaths with weaker shocks. There is, however, considerable event-to-event variation in flux profiles for both categories.

The proton measurements averaged over approximately corresponding energy ranges are shown in the right columns of Fig. 6 for the PSP 30 June 2021 event studied previously in this paper. Evidently, the profile is atypical when compared to most of the ACE events, in particular strong M_{ms} cases that mostly show declining intensity profiles through the sheath.

4 Discussion

The details of energization of charged particles related to CMEs/ICMEs remains partly an open question in solar-terrestrial research. As discussed in the Introduction, DSA is considered the key mechanism for accelerating ions at coronal and interplanetary shocks, but there are several mechanisms presented in the literature relevant to how sheaths could contribute to the energization.

For the investigated event the enhancement of energetic protons started about an hour after the passage of the leading ICME shock. This is interesting as the shock was estimated to be strong and quasi-parallel. However, the driving ICME was slow with the peak speed only ~ 400 km/s and it was able to drive a shock as the upstream Alfvén speed was very low. Another prominent feature in the studied event was that the energetic proton fluxes stayed elevated throughout the sheath. These features imply that some mechanism internal to the sheath was responsible for the observed energization.

One possible scenario is that particles gain energy via first-order Fermi acceleration while entering in a global compression region (e.g., Schwadron et al. 2020; Giacalone et al. 2002). The sheath investigated in this study had a very high density (up to 50 cm^{-3}) and the density increased gradually from the shock to the magnetic cloud leading edge. This mechanism has been suggested to be an important contributor in particle energization in SIRs rather than acceleration at the associated forward and reverse shocks (e.g., Giacalone et al. 2002).

The energetic proton fluxes had, however, large and sporadic variations throughout the sheath, suggesting that the

acceleration could have occurred in an intermittent manner. Another possibility is that magnetic disturbances in the sheath accelerate particles stochastically, i.e. via second-order Fermi acceleration (e.g., Richardson 1985). This is less effective as the process involves both head-on and tail-on collisions. The sheath embedded enhanced levels of magnetic field fluctuations compared to the upstream wind at various time scales. The positive correlation of ~ 0.4 between normalized fluctuation amplitudes and proton flux variations at larger time scales across a wide range of energies could imply that fluctuations contributed to the energization. The highest positive correlations occurred for fluctuations $\gtrsim 100$ seconds.

Particles can be accelerated stochastically with gyroresonant Alfvén waves (e.g., Afanasiev et al. 2014). The gyroresonance condition assuming Taylor hypothesis and radial wave vector and solar wind flow can be written as

$$f_{res} = f_g \frac{V_{sw}}{|v\mu|},$$

where f_{res} is the resonant frequency of the magnetic field fluctuation in the spacecraft frame, V_{sw} is the solar wind speed, f_g is the gyrofrequency and, v is the speed of the resonant particle and μ the cosine of the pitch angle of that particle. Using the average values in the sheath, $B = 10$ nT, $V_{sw} = 360$ km/s and field aligned particles ($\mu = 1$) gives for 100 keV protons the resonant fluctuation timescale ~ 80 seconds and for 150 keV protons ~ 100 seconds. This is a rough estimate, but corresponds to approximately the start of the higher correlation in the left part of Fig. 5. We however note that the high correlations occur over a wider range of time lags and peak around 500 seconds. This could be explained by the magnetic field not being radial in the sheath. Another possibility is that the resonance is with compressive magnetosonic waves. In that case transit-time damping should dominate (e.g., Schwadron et al. 1996; Schlickeiser and Vainio 1999).

Our study also revealed a positive correlation of ~ 0.4 between proton flux variation and the occurrence of periods of highly reduced magnetic helicity in the sheath. It is therefore possible that the related structures can contribute to the energization. Intervals of high reduced magnetic helicity can represent either small-scale flux ropes that can energize ions as they get compressed into the sheath (e.g., Kilpua et al. 2021b; Trotta et al. 2022a) or Alfvén waves that can act as scattering centers for second-order Fermi acceleration (e.g., Vainio and Afanasiev 2018). Without good quality plasma data we cannot distinguish between these.

The statistical analysis of ion intensities observed during 73 sheaths by the ACE spacecraft confirms that sheaths may in general have an important contribution to energization. In particular, the effect was clear for sheaths behind weak shocks. It will be interesting in the future to repeat a

statistical analysis using observations closer to the Sun than 1 AU using a combination of PSP, Solar Orbiter and Bepi-Colombo measurements as particle acceleration is expected to be more effective at these distances. A more detailed analysis is also needed to investigate how ion/proton profiles depend on sheath properties and internal structure.

5 Conclusion

In this paper we have investigated a peculiar energetic proton enhancement that occurred up to ~ 300 keV related to a sheath region ahead of a slow ICME. The event was observed by PSP at 0.76 AU on June 30 – July 1, 2022. Despite the ICME being slow, it drove a strong shock wave ahead of it. The energetic proton enhancement commenced about one hour after the shock. The fluxes had a sporadic nature, but stayed enhanced throughout the sheath. Based on a statistical analysis of shocks detected at 1 AU, the energetic ion fluxes tend to typically peak at the shock and then decline. The investigated event resembled more the behaviour associated with weak shocks. The possible energization mechanism in the studied sheath is likely a combination of compressional acceleration and acceleration by Alfvénic fluctuations or small-scale structures embedded in the sheath.

Acknowledgements This study has received funding through the European Union's Horizon 2020 research and innovation programme under grant agreement No 101004159 (SERPENTINE). EK acknowledges the ERC under the European Union's Horizon 2020 Research and Innovation Programme Project 724391 (SolMAG). The US authors were supported as a part of the PSP mission under contract NNN06AA01C. Work in the University of Turku and University of Helsinki was performed under the umbrella of Finnish Centre of Excellence in Research of Sustainable Space (Academy of Finland Grant no. 336809, 312390 and 336809). Parker Solar Probe was designed, built, and is now operated by the Johns Hopkins Applied Physics Laboratory as part of NASA's Living with a Star (LWS) program (contract NNN06AA01C). ND is grateful for support by the Academy of Finland (SHOCKSEE, grant No. 346902).

Author contributions E. Kilpua was the primary responsible of the data analysis. All authors have been contributing to the writing and interpretation of the analysis in the paper.

Funding Note Open Access funding provided by University of Helsinki including Helsinki University Central Hospital.

Declarations

Competing interests The authors declare no competing interests.

Open Access This article is licensed under a Creative Commons Attribution 4.0 International License, which permits use, sharing, adaptation, distribution and reproduction in any medium or format, as long as you give appropriate credit to the original author(s) and the source, provide a link to the Creative Commons licence, and indicate if changes were made. The images or other third party material in this article are included in the article's Creative Commons licence, unless indicated

otherwise in a credit line to the material. If material is not included in the article's Creative Commons licence and your intended use is not permitted by statutory regulation or exceeds the permitted use, you will need to obtain permission directly from the copyright holder. To view a copy of this licence, visit <http://creativecommons.org/licenses/by/4.0/>.

References

- Afanasiev, A., Vainio, R., Kocharov, L.: The effect of stochastic re-acceleration on the energy spectrum of shock-accelerated protons. *Astrophys. J.* **790**(1), 36 (2014). <https://doi.org/10.1088/0004-637X/790/1/36>
- Afanasiev, A., Battarbee, M., Vainio, R.: Self-consistent Monte Carlo simulations of proton acceleration in coronal shocks: effect of anisotropic pitch-angle scattering of particles. *Astron. Astrophys.* **584**, A81 (2015). <https://doi.org/10.1051/0004-6361/201526750>. [arXiv:1603.08857](https://arxiv.org/abs/1603.08857) [physics.space-ph]
- Afanasiev, A., Vainio, R., Rouillard, A.P., et al.: Modelling of proton acceleration in application to a ground level enhancement. *Astron. Astrophys.* **614**, A4 (2018). <https://doi.org/10.1051/0004-6361/201731343>. [arXiv:1806.05497](https://arxiv.org/abs/1806.05497) [astro-ph.SR]
- Bale, S.D., Goetz, K., Harvey, P.R., et al.: The FIELDs instrument suite for solar probe plus. Measuring the coronal plasma and magnetic field, plasma waves and turbulence, and radio signatures of solar transients. *Space Sci. Rev.* **204**(1–4), 49–82 (2016). <https://doi.org/10.1007/s11214-016-0244-5>
- Burlaga, L., Sittler, E., Mariani, F., et al.: Magnetic loop behind an interplanetary shock: Voyager, Helios, and IMP 8 observations. *J. Geophys. Res.* **86**(A8), 6673–6684 (1981). <https://doi.org/10.1029/JA086iA08p06673>
- Desai, M., Giacalone, J.: Large gradual solar energetic particle events. *Living Rev. Sol. Phys.* **13**(1), 3 (2016). <https://doi.org/10.1007/s41116-016-0002-5>
- Fox, N.J., Velli, M.C., Bale, S.D., et al.: The Solar Probe Plus mission: humanity's first visit to our star. *Space Sci. Rev.* **204**(1–4), 7–48 (2016). <https://doi.org/10.1007/s11214-015-0211-6>
- Giacalone, J.: Energetic charged particles associated with strong interplanetary shocks. *Astrophys. J.* **761**(1), 28 (2012). <https://doi.org/10.1088/0004-637X/761/1/28>
- Giacalone, J., Jokipii, J.R., Kóta, J.: Particle acceleration in solar wind compression regions. *Astrophys. J.* **573**(2), 845–850 (2002). <https://doi.org/10.1086/340660>
- Giacalone, J., Mitchell, D.G., Allen, R.C., et al.: Solar energetic particles produced by a slow coronal mass ejection at ~ 0.25 au. *Astrophys. J. Suppl. Ser.* **246**(2), 29 (2020). <https://doi.org/10.3847/1538-4365/ab5221>
- Gold, R.E., Krimigis, S.M., Hawkins III, S.E., et al.: Electron, proton, and alpha monitor on the advanced composition explorer spacecraft. *Space Sci. Rev.* **86**, 541–562 (1998). <https://doi.org/10.1023/A:1005088115759>
- Hietala, H., Laitinen, T.V., Andréová, K., et al.: Supermagnetosonic jets behind a collisionless quasiparallel shock. *Phys. Rev. Lett.* **103**(24), 245001 (2009). <https://doi.org/10.1103/PhysRevLett.103.245001>. [arXiv:0911.1687](https://arxiv.org/abs/0911.1687) [physics.plasm-ph]
- Hill, M.E., Mitchell, D.G., Andrews, G.B., et al.: The mushroom: a half-sky energetic ion and electron detector. *J. Geophys. Res. Space Phys.* **122**(2), 1513–1530 (2017). <https://doi.org/10.1002/2016JA022614>
- Hill, M.E., Mitchell, D.G., Allen, R.C., et al.: Small, low-energy, dispersive solar energetic particle events observed by Parker Solar Probe. *Astrophys. J. Suppl. Ser.* **246**(2), 65 (2020). <https://doi.org/10.3847/1538-4365/ab643d>
- Kajdič, P., Preisser, L., Blanco-Cano, X., et al.: First observations of irregular surface of interplanetary shocks at ion scales by cluster.

- Astrophys. J. Lett. **874**(2), L13 (2019). <https://doi.org/10.3847/2041-8213/ab0e84>. arXiv:1903.11653 [physics.space-ph]
- Kajdič, P., Pfau-Kempf, Y., Turc, L., et al.: Ulf wave transmission across collisionless shocks: 2.5d local hybrid simulations. *J. Geophys. Res. Space Phys.* **A029**, 283 (2021). <https://doi.org/10.1029/2021JA029283>. <https://agupubs.onlinelibrary.wiley.com/doi/abs/10.1029/2021JA029283>.
- Kasper, J.C., Abiad, R., Austin, G., et al.: Solar Wind Electrons Alphas and Protons (SWEAP) investigation: design of the solar wind and coronal plasma instrument suite for Solar Probe Plus. *Space Sci. Rev.* **204**(1–4), 131–186 (2016). <https://doi.org/10.1007/s11214-015-0206-3>
- Kilpua, E.K.J., Lumme, E., Andreeva, K., et al.: Properties and drivers of fast interplanetary shocks near the orbit of the Earth (1995–2013). *J. Geophys. Res. Space Phys.* **120**(6), 4112–4125 (2015). <https://doi.org/10.1002/2015JA021138>
- Kilpua, E., Koskinen, H.E.J., Pulkkinen, T.I.: Coronal mass ejections and their sheath regions in interplanetary space. *Living Rev. Sol. Phys.* **14**, 5 (2017). <https://doi.org/10.1007/s41116-017-0009-6>
- Kilpua, E.K.J., Fontaine, D., Moissard, C., et al.: Solar wind properties and geospace impact of coronal mass ejection-driven sheath regions: variation and driver dependence. *Space Weather* **17**(8), 1257–1280 (2019). <https://doi.org/10.1029/2019SW002217>
- Kilpua, E.K.J., Fontaine, D., Good, S.W., et al.: Magnetic field fluctuation properties of coronal mass ejection-driven sheath regions in the near-Earth solar wind. *Ann. Geophys.* **38**(5), 999–1017 (2020). <https://doi.org/10.5194/angeo-38-999-2020>
- Kilpua, E.K.J., Good, S.W., Ala-Lahti, M., et al.: Statistical analysis of magnetic field fluctuations in CME-driven sheath regions. *Front. Astron. Space Sci.* **7**, 109 (2021a). <https://doi.org/10.3389/fspas.2020.610278>
- Kilpua, E.K.J., Good, S.W., Dresing, N., et al.: Multi-spacecraft observations of the structure of the sheath of an interplanetary coronal mass ejection and related energetic ion enhancement. *Astron. Astrophys.* **656**, A8 (2021b). <https://doi.org/10.1051/0004-6361/202140838>. arXiv:2112.09472 [physics.space-ph]
- Kouloumvakos, A., Rouillard, A.P., Wu, Y., et al.: Connecting the properties of coronal shock waves with those of solar energetic particles. *Astrophys. J.* **876**(1), 80 (2019). <https://doi.org/10.3847/1538-4357/ab15d7>
- Krivolutsky, A.A., Repnev, A.I.: Impact of space energetic particles on the Earth's atmosphere (a review). *Geomagn. Aeron.* **52**(6), 685–716 (2012). <https://doi.org/10.1134/S0016793212060060>
- Manchester IV, W.B., Gombosi, T.I., De Zeeuw, D.L., et al.: Coronal mass ejection shock and sheath structures relevant to particle acceleration. *Astrophys. J.* **622**(2), 1225–1239 (2005). <https://doi.org/10.1086/427768>
- Matthaeus, W., Goldstein, M., Smith, C.: Evaluation of magnetic helicity in homogeneous turbulence. *Phys. Rev. Lett.* **48**(18), 1256–1259 (1982). <https://doi.org/10.1103/PhysRevLett.48.1256>
- McComas, D.J., Alexander, N., Angold, N., et al.: Integrated Science Investigation of the Sun (ISIS): design of the energetic particle investigation. *Space Sci. Rev.* **204**(1–4), 187–256 (2016). <https://doi.org/10.1007/s11214-014-0059-1>
- Preisser, L., Blanco-Cano, X., Trotta, D., et al.: Influence of He⁺⁺ and shock geometry on interplanetary shocks in the solar wind: 2D hybrid simulations. *J. Geophys. Res. Space Phys.* **A027**, 442 (2020). <https://doi.org/10.1029/2019JA027442>. <https://agupubs.onlinelibrary.wiley.com/doi/abs/10.1029/2019JA027442>
- Reames, D.V.: The two sources of solar energetic particles. *Space Sci. Rev.* **175**(1–4), 53–92 (2013). <https://doi.org/10.1007/s11214-013-9958-9>. arXiv:1306.3608 [astro-ph.SR]
- Retinò, A., Khotyaintsev, Y., Le Contel, O., et al.: Particle energization in space plasmas: towards a multi-point, multi-scale plasma observatory. *Exp. Astron.* (2021). <https://doi.org/10.1007/s10686-021-09797-7>
- Richardson, I.G.: low energy ions in co-rotating interaction regions at 1 AU: evidence for statistical ion acceleration. *Planet. Space Sci.* **33**(5), 557–569 (1985). [https://doi.org/10.1016/0032-0633\(85\)90097-2](https://doi.org/10.1016/0032-0633(85)90097-2)
- Richardson, I.G.: Solar wind stream interaction regions throughout the heliosphere. *Living Rev. Sol. Phys.* **15**(1), 1 (2018). <https://doi.org/10.1007/s41116-017-0011-z>
- Ruohotie, J., Kilpua, E.K.J., Good, S.W., et al.: Small-scale flux ropes in ICME sheaths. *Front. Astron. Space Sci.* **9**, 943247 (2022). <https://doi.org/10.3389/fspas.2022.943247>. arXiv:2208.07662 [physics.space-ph]
- Schlickeiser, R., Vainio, R.: Recent developments in quasilinear cosmic ray particle acceleration theories. *Astrophys. Space Sci.* **264**, 457–469 (1999). <https://doi.org/10.1023/A:1002462508325>
- Schwadron, N.A., Fisk, L.A., Gloeckler, G.: Statistical acceleration of interstellar pick-up ions in co-rotating interaction regions. *Geophys. Res. Lett.* **23**(21), 2871–2874 (1996). <https://doi.org/10.1029/96GL02833>
- Schwadron, N.A., Bale, S., Bonnell, J., et al.: Seed population preconditioning and acceleration observed by the Parker Solar Probe. *Astrophys. J. Suppl. Ser.* **246**(2), 33 (2020). <https://doi.org/10.3847/1538-4365/ab5527>. arXiv:1912.02888 [astro-ph.SR]
- Stone, E.C., Frandsen, A.M., Mewaldt, R.A., et al.: The advanced composition explorer. *Space Sci. Rev.* **86**, 1–22 (1998). <https://doi.org/10.1023/A:1005082526237>
- Sundberg, T., Haynes, C.T., Burgess, D., et al.: Ion acceleration at the quasi-parallel bow shock: decoding the signature of injection. *Astrophys. J.* **820**(1), 21 (2016). <https://doi.org/10.3847/0004-637X/820/1/21>. arXiv:1511.02077 [astro-ph.HE]
- Trotta, D., Burgess, D.: Electron acceleration at quasi-perpendicular shocks in sub- and supercritical regimes: 2D and 3D simulations. *Mon. Not. R. Astron. Soc.* **482**(1), 1154–1162 (2019). <https://doi.org/10.1093/mnras/sty2756>
- Trotta, D., Pecora, F., Settino, A., et al.: On the transmission of turbulent structures across the Earth's bow shock. *Astrophys. J.* **933**(2), 167 (2022a). <https://doi.org/10.3847/1538-4357/ac7798>
- Trotta, D., Vuorinen, L., Hietala, H., et al.: Single-spacecraft techniques for shock parameters estimation: a systematic approach. *Front. Astron. Space Sci.* **9**, 1005672 (2022b). <https://doi.org/10.3389/fspas.2022.1005672>. <https://www.frontiersin.org/articles/10.3389/fspas.2022.1005672>
- Vainio, R., Afanasiev, A.: Particle acceleration mechanisms. In: Malandraki, O.E., Crosby, N.B. (eds.) *Solar Particle Radiation Storms Forecasting and Analysis*, pp. 45–61 (2018). https://doi.org/10.1007/978-3-319-60051-2_3
- Vainio, R., Desorgher, L., Heynderickx, D., et al.: Dynamics of the Earth's particle radiation environment. *Space Sci. Rev.* **147**(3–4), 187–231 (2009). <https://doi.org/10.1007/s11214-009-9496-7>
- Webb, D.F., Howard, T.A.: Coronal mass ejections: observations. *Living Rev. Sol. Phys.* **9**(1), 3 (2012). <https://doi.org/10.12942/lrsp-2012-3>
- Zhao, L.L., Zank, G.P., Adhikari, L., et al.: Identification of magnetic flux ropes from Parker Solar Probe observations during the first encounter. *Astrophys. J. Suppl. Ser.* **246**(2), 26 (2020). <https://doi.org/10.3847/1538-4365/ab4ff1>. arXiv:1912.02349 [physics.space-ph]
- Zhao, L.L., Zank, G.P., Hu, Q., et al.: Detection of small magnetic flux ropes from the third and fourth Parker Solar Probe encounters. *Astron. Astrophys.* **650**, A12 (2021). <https://doi.org/10.1051/0004-6361/202039298>. arXiv:2010.04664 [astro-ph.SR]

Publisher's Note Springer Nature remains neutral with regard to jurisdictional claims in published maps and institutional affiliations.

Authors and Affiliations

Emilia Kilpua¹ · Rami Vainio² · Christina Cohen³ · Nina Dresing² · Simon Good¹ · Julia Ruohotie¹ · Domenico Trotta⁴ · Stuart D. Bale⁵ · Eric Christian⁶ · Matt Hill⁷ · David J. McComas⁸ · Ralph McNutt⁷ · Nathan Schwadron⁹

✉ E. Kilpua
emilia.kilpua@helsinki.fi

R. Vainio
rami.vainio@utu.fi

C. Cohen
cohen@srl.caltech.edu

N. Dresing
nina.dresing@utu.fi

S. Good
simon.good@helsinki.fi

J. Ruohotie
julia.ruohotie@helsinki.fi

D. Trotta
d.trotta@imperial.ac.uk

S.D. Bale
bale@ssl.berkeley.edu

E. Christian
eric.r.christian@nasa.gov

M. Hill
Matthew.Hill@jhuapl.edu

D.J. McComas
dmccomas@princeton.edu

R. McNutt
ralph.mcnutt@jhuapl.edu

N. Schwadron
Nathan.Schwadron@unh.edu

¹ Department of Physics, University of Helsinki, P.O. Box 64, Helsinki, FI-00014, Finland

² Department of Physics and Astronomy, University of Turku, Turku, FI-20014, Finland

³ Space Radiation Lab, California Institute of Technology, MC 290-17, Pasadena, 91125, California, USA

⁴ The Blackett Laboratory, Department of Physics, Imperial College London, London, SW7 2AZ, UK

⁵ Physics Department and Space Sciences Laboratory, University of California, Berkeley, California, USA

⁶ NASA Goddard Space Flight Center, Greenbelt, 20771, MD, USA

⁷ Applied Physics Laboratory, Johns Hopkins University, Laurel, 20723, Maryland, USA

⁸ Department of Astrophysical Sciences, Princeton University, Princeton, New Jersey, 08544, USA

⁹ University of New Hampshire, Durham, New Hampshire, USA